



A mid-Cretaceous enantiornithine (Aves) hatchling preserved in Burmese amber with unusual plumage



Lida Xing^{a,b,1}, Jingmai K. O'Connor^{c,*,1}, Ryan C. McKellar^{d,e,f,1}, Luis M. Chiappe^{g,1}, Kuowei Tseng^h, Gang Liⁱ, Ming Bai^{j,*,1}

^a State Key Laboratory of Biogeology and Environmental Geology, China University of Geosciences, Beijing 100083, China

^b School of the Earth Sciences and Resources, China University of Geosciences, Beijing 100083, China

^c Key Laboratory of Vertebrate Evolution and Human Origins of the Chinese Academy of Sciences, Institute of Vertebrate Paleontology and Paleoanthropology, Beijing 100044, China

^d Royal Saskatchewan Museum, Regina, Saskatchewan S4P 4W7, Canada

^e Biology Department, University of Regina, Regina, Saskatchewan S4S 0A2, Canada

^f Department of Ecology & Evolutionary Biology, 1501 Crestline Drive – Suite 140, University of Kansas, Lawrence, KS 66045, USA

^g Dinosaur Institute, Natural History Museum of Los Angeles County, 900 Exposition Boulevard, Los Angeles, CA 90007, USA

^h Department of Exercise and Health Science, University of Taipei, Taipei 11153, China

ⁱ Institute of High Energy Physics, Chinese Academy of Science, 19B Yuquan Rd., Beijing 100049, China

^j Key Laboratory of Zoological Systematics and Evolution, Institute of Zoology, Chinese Academy of Sciences, Box 92, Beichen West Road, Chaoyang District, Beijing 100101, China

ARTICLE INFO

Article history:

Received 23 January 2017

Received in revised form 17 May 2017

Accepted 2 June 2017

Available online 06 June 2017

Handling Editor: I. Somerville

Keywords:

Enantiornithes

Juvenile

Osteology

Plumage

Soft tissue preservation

ABSTRACT

Burmese amber has recently provided some detailed glimpses of plumage, soft tissues, and osteology of juvenile enantiornithine birds, but these insights have been restricted to isolated wing apices. Here we describe nearly half of a hatchling individual, based on osteological and soft tissue data obtained from the skull, neck, feet, and wing, and identified as a member of the extinct avian clade Enantiornithes. Preserved soft tissue provides the unique opportunity to observe the external opening of the ear, the eyelid, and fine details of tarsal scutellation. The new amber specimen yields the most complete view of hatchling plumage and integument yet to be recovered from the Cretaceous, including details of pterylosis, feather microstructure, and pigmentation patterns. The hatchling was encapsulated during the earliest stages of its feather production, providing a point for comparisons to other forms of body fossils, as well as isolated feathers found in Cretaceous ambers. The plumage preserves an unusual combination of precocial and altricial features unlike any living hatchling bird, having functional remiges combined with sparse body feathers. Unusual feather morphotypes on the legs, feet, and tail suggest that first generation feathers in the Enantiornithes may have been much more like contour feathers than the natal down observed in many modern birds. However, these regions also preserve filamentous feathers that appear comparable to the protofeathers observed in more primitive theropods. Overall, the new specimen brings a new level of detail to our understanding of the anatomy of the juvenile stages of the most species-rich clade of pre-modern birds and contributes to mounting data that enantiornithine development drastically differed from that of Neornithes.

© 2017 International Association for Gondwana Research. Published by Elsevier B.V. All rights reserved.

1. Introduction

Besides traditionally preserved dinosaur skeletal fossils—including birds—examples of exceptional preservation provide fundamental information for understanding the biology of these animals as in the ‘mummified’ hadrosaurids *Edmontosaurus* (Osborn, 1912) and *Brachylophosaurus* (Murphy et al., 2006), the coelurosaurian *Scipionyx* (Dal Sasso and Signore, 1998), and numerous fossils from the Jehol fauna (Zhou et al., 2003; Xing et al., 2012), which preserve integumentary structures as

well as internal organs (Zheng et al., 2013). Despite their exceptional contribution to dinosaur paleobiology, these fossils are regularly impacted by diagenesis and other taphonomic factors that obscure some aspects of these structures from full scrutiny. The previous fossil record of juvenile and embryonic enantiornithines, a diverse clade of pre-modern birds, is no exception. Well-preserved specimens have been reported from Cretaceous sites in China (Zhou and Zhang, 2004; Chiappe et al., 2007), Mongolia (Elzanowski, 1981), Spain (Sanz et al., 1997, 2001), Argentina (Schweitzer et al., 2002) and Brazil (de Souza Carvalho et al., 2015). However, in compressed fossils preserved integumentary structures consist of partially preserved precocial remiges, tufted dorsal plumage traces, or elongate tail feathers. Only one previous juvenile specimen has preserved feathers with any significant relief (de Souza Carvalho et al., 2015).

* Corresponding authors.

E-mail addresses: jingmai@ivpp.ac.cn (J.K. O'Connor), baim@ioz.ac.cn (M. Bai).

¹ These authors contributed equally to this work.

Amber offers unmatched preservation, but is severely limited in the size of the inclusions that it preserves (Martínez-Delclòs et al., 2004). Burmese amber is exceptional among the Cretaceous amber deposits, in that the pieces are relatively, large, clear, and durable, and the deposit has been mined on a massive scale (S. Wang et al., 2016). Within the last twenty years, Cretaceous sites in northern Myanmar have become paramount for the study of fossil insects and plants trapped within amber, and recently these deposits have become increasingly important in the study of vertebrates (Daza et al., 2016). We have been studying vertebrate materials from Myanmar since 2014, including two enantiornithine wings (Xing et al., 2016a) and the tail of a non-avian coelurosaurian theropod (Xing et al., 2016b). Here we describe another piece of Burmese amber that includes the head, cervical vertebrae, wings, and feet of an enantiornithine bird, as well as a considerable amount of associated soft tissue and integumentary structures (Fig. 1).

Based on biostratigraphic evidence (ammonites and palynology), the Cretaceous Burmese amber has been assigned a late Albian–Cenomanian age (about 105 to 95 million years old) (Cruickshank and Ko, 2003; Ross et al., 2010). U–Pb dating of zircons from the volcanoclastic matrix of the amber gives a refined age estimate of

approximately 98.8 ± 0.6 million years for the deposit (Shi et al., 2012). This amber is thought to be the product of a conifer, perhaps belonging to the Cupressaceae or Araucariaceae, that once lived in a moist tropical setting (Grimaldi et al., 2002; Ross et al., 2010).

2. Material and methods

2.1. Material and photography

The new specimen, HPG-15-1, comes from the Angbamo site, Tanai Township (Myitkyina District, Kachin Province) of northern Myanmar. It measures approximately 86 mm × 30 mm × 57 mm, weighs 78.16 g, and is cut through the middle into two sections. The original specimen is housed and displayed in the Hupoge Amber Museum (= HPG), Tengchong City Amber Association, China; the 3D printing models are available to researchers through the Institute of Zoology, CAS and the Dexu Institute of Palaeontology (= DIP), China.

The two pieces of amber forming HPG-15-1 were examined with a Leica MZ 12.5 dissecting microscope with a drawing tube attachment. Photographs were taken using a Canon digital camera (5D Mark III,

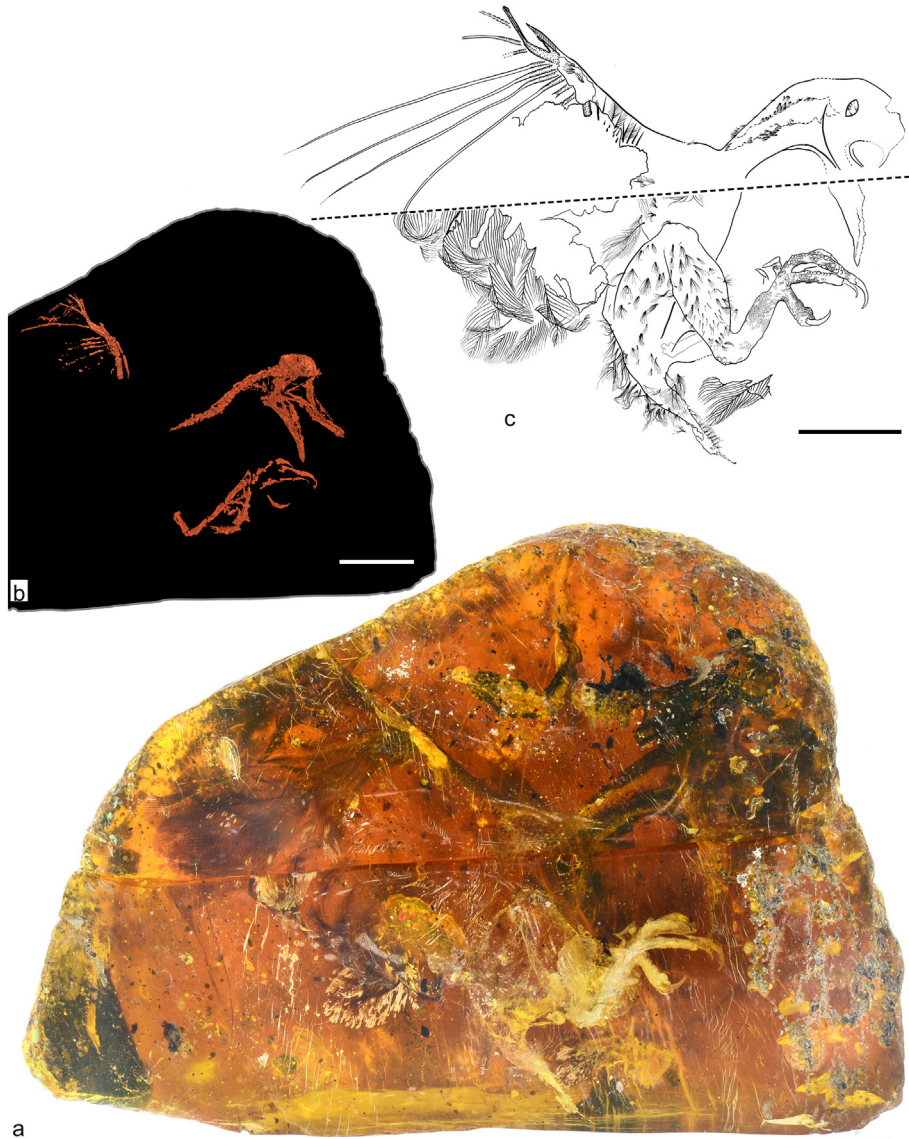


Fig. 1. Overview of HPG-15-1 in right lateral view. a, amber specimen; b, X-ray μ CT reconstruction; c, illustration of observable plumage and skin sections. Two halves of amber piece have been positioned side by side (a) or separated by dashed line (c), and body regions scanned separately have been arranged in preservational position (b). For clarity in (c), only rachises of apical remiges indicated; and only rachises and rami of basal remiges, coverts, contours, and neoptile plumage indicated. Scale bars represent 10 mm.

MP-E 65MM F/2.8 1–5×) fitted to a macro rail (Cognisys), and were processed using Helicon Focus 5.1 and Adobe Photoshop CS5 software to increase depth of field in the images. These images were supplemented with photos taken under long wavelength UV light, mapping resin flows.

2.2. Micro-CT scanning and 3D reconstruction

HPG-15-1 was scanned with a MicroXCT 400 (Carl Zeiss X-ray Microscopy, Inc., Pleasanton, USA) at the Institute of Zoology, Chinese Academy of Sciences, Beijing. A single scan of the entire piece was not possible due to its large size. The different parts of the bird were scanned separately. The head, neck, wing, and hind limbs, were scanned with a beam strength of 60 kV, and an absorption contrast and a spatial resolution of 18.3298 μm, 18.3298 μm, 3.7795 μm, and 25.5308 μm, respectively.

Based on the obtained image stacks, structures of the specimen were reconstructed and isolated using Amira 5.4 (Visage Imaging, San Diego, USA). The subsequent volume rendering and animations were performed using VG Studiomax 2.1 (Volume Graphics, Heidelberg, Germany). Final figures were prepared with Photoshop CS5 (Adobe, San Jose, USA) and Illustrator CS5 (Adobe, San Jose, USA).

2.3. Integumentary structure terminology

Within our descriptive work, the feather and skin terminology presented by Lucas and Stettenheim (1972) is largely followed. Supplemental details related to barbule morphology and pigmentation follow Dove (2000).

There are two distinct forms of neoptile feathers present across multiple body regions in the studied specimen: the first morphotype matches well with the down feathers of modern birds, with elongate (plumulaceous) barbules, flexible barbs, and a poorly defined rachis; the second morphotype is widespread on the body, shares the flattened (pennaceous) barb arrangement, and short rachis seen in modern neoptile feathers (*sensu* Foth, 2011), but the barbs bear barbules that are pennaceous in form and would be classified as contour feathers (*sensu* Lucas and Stettenheim, 1972). For the sake of brevity, the first morphotype will be referred to as ‘down’ or ‘plumulaceous feathers’, and the second morphotype will simply be referred to as ‘neoptile’ plumage in subsequent sections.

3. Results

3.1. Osteological characters

3.1.1. Skull

Unfortunately, the skull was split when the amber was cut (Figs. 1c; 2a–d). The rostrum is preserved in one section and the neck and most of the braincase in the other. The thinner, more delicate bones of the skull are not clear in the X-ray μCT scan, and the right jugal is crushed inwards. The skull is mesorostrine, with the length of the rostrum being approximately the same as the length of the postrostral region. The rostral ends of the facial margin of both the upper and lower jaws are jagged. This is most pronounced on the premaxilla and rostrally restricted on the dentary and could represent remnants of a horny beak or small teeth. A single tooth is clearly visible in the left premaxilla (Fig. 2a, b). The tooth has a bulbous crown that rapidly tapers apically and a strong basal constriction, a morphology common in early birds. The premaxillary corpus appears fairly short, as in Early Cretaceous enantiornithines, forming approximately one-third of the rostrum. It is medially fused as in enantiornithine embryos from Mongolia (Elzanowski, 1981; Kurochkin et al., 2013). In rostral view the tips of the premaxillae ventrally define a 60° angle, a condition also observed in the adults of the enantiornithine *Gobipteryx* (Kurochkin, 1996; Chiappe et al., 2001). The frontal processes of the premaxillae appear to be elongate, reaching

the frontals (not reaching in some basal enantiornithines), connecting medially by a suture (not visible in ventral view). The maxillae and nasals are represented by numerous fragments, which indicate that the nares and antorbital fenestra were separated, although it is unclear whether by an extension of the nasal (as in *Gobipteryx*), the maxilla, or both (O'Connor and Chiappe, 2011). The ventral surface of the right maxilla is concave, with a well-developed tomial margin without any visible teeth or alveoli. The premaxillary process of the maxilla appears to form a complex, forked articulation with the premaxilla similar to *Gobipteryx* (Chiappe et al., 2001). The vomerine process is short and bluntly tapered, and it appears to articulate with a portion of the vomers. The jugal process of the maxilla is elongate, lacking a caudomedial process (perhaps not preserved). Fragments of the lacrimal appear to be preserved on the left side. The maxilla articulates with the jugal laterally. The jugal is straight and mediolaterally compressed (strap-like). The separate quadratojugal is rod-like and dorsally concave; it articulates with the jugal dorsomedially for more than half of its length (Fig. 2b). A distinct squamosal ramus like that present in some other enantiornithines is absent (M. Wang et al., 2016). The palatal bones are fragmentary. A ventrally facing plate-like bone preserved at the cranial hinge is identified as the parasphenoid. A narrow, elongate bone extends from the midline of this bone cranially to the level of the rostral margin of the orbit and is tentatively identified as the parasphenoid rostrum. A similar bone located between the parasphenoid rostrum and jugal is unidentified. Alternatively, these two bones could constitute portions of the hyoids. The morphology of the quadrate is unclear on both sides (split on the right and possibly disarticulated on the left).

The occipital bones appear unfused medially. The dorsally convex frontals are very narrow rostrally. Their rostral ends are slightly slanted ventromedially-dorsolaterally, defining a medial furrow, which may be exaggerated by some mediolateral crushing of the skull. The frontals articulate for most of their length with a small gap between their rostral ends as in *Archaeopteryx* (Mayr et al., 2007). The caudal portions of the frontals are greatly expanded. A crest defines their caudal articulation with the parietals. It appears that a sagittal crest may also have been present. The caudally oriented foramen magnum is large and taller than wide. The occipital condyle is obscured by articulation with the cervical vertebrae. However, the interior surface indicates that the exoccipitals contributed to the dorsal portion of the condyle and were unfused at the time of death, as in known Early Cretaceous enantiornithines (O'Connor and Chiappe, 2011). The supraoccipital bears a strong cerebral prominence. The paraoccipital processes are well-developed. Features such as the oval morphology of the foramen magnum and the size of the cerebral prominence and sagittal crest may be exaggerated by mediolateral compression of the cranium. Visible from the interior surface of the parietals, a ventral depression may represent the pineal fossa; this feature is not obvious externally, similar to *Archaeopteryx* (Alonso et al., 2004). The inner ear and its semicircular canals are partially preserved on the left; this region is shrouded in a mass of tissue on the right. The anterior and posterior semicircular canals are visible; the former is much larger than the latter. These are connected to the cochlea, which does not preserve anatomical data.

The tip of the mandible is slightly downturned (Fig. 2a–d). The contacts between mandibular bones are unclear suggesting some degree of fusion, although this is incongruent with the apparent lack of fusion in the braincase and the very young age inferred for the specimen; this suggests that here and other apparent instances of fusion in the cranium may be taphonomic. As in other enantiornithines, the splenials do not reach the mandibular symphysis (O'Connor and Chiappe, 2011), which is well-developed, extending along the rostral fifth of the mandible, similar to *Gobipteryx* but unlike Jehol enantiornithines in which the dentaries are unfused and inferred to have a short rostral articulation.

3.1.2. Neck

There are at least six articulated cervical vertebrae from HPG-15-1, including the atlas and axis, preserved in articulation with the skull

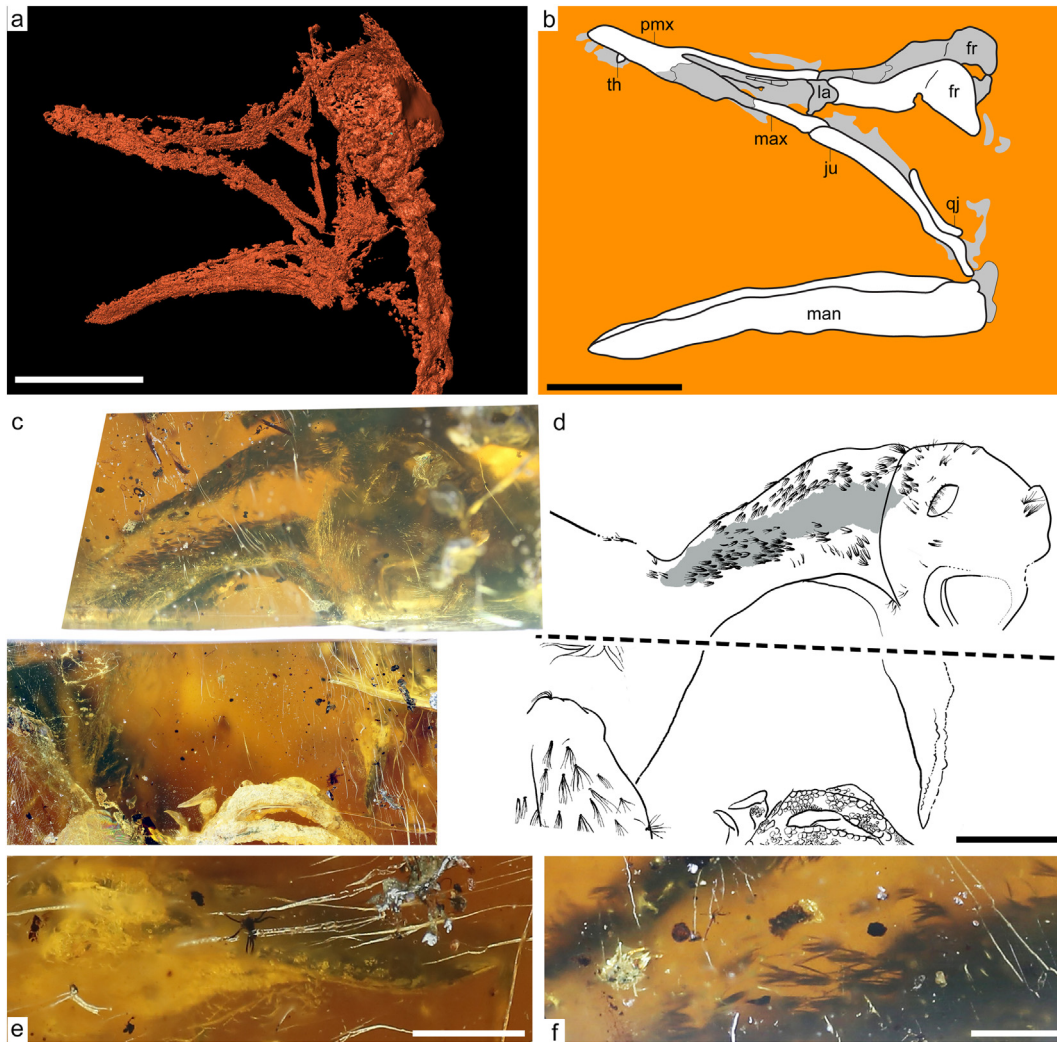


Fig. 2. Details of the head in HPG-15-1. a, X-ray μ CT reconstruction in left lateral view; b, interpretative drawing of the skull based on X-ray μ CT reconstructions; c, detailed view of head and neck, of visible plumage and integumentary structures, with only distinct (not strongly overlapping) feathers indicated, grey area depicting area of apterium and lower-density plumage, barbules omitted within neoptile plumage of hind limb, and dorsal rostrum omitted due to lack of clear view; d, corresponding illustration to panel (c); e, detailed view of dentary; f, detailed view of feathers bordering cervical apterium. Abbreviation scheme: fr (frontal); ju (jugal); la (lacrimal); man (mandible); max (maxilla); pmx (premaxilla); qj (quadratojugal); th (tooth). Scale bars equal 5 mm in (a–d), 1 mm in (e–f).

(Fig. 1b). The atlantal hemi-arches appear to be unfused dorsally, but it cannot be determined if they are also unfused to the centrum. The axis is short, wider than long and wider caudally than cranially. The dorsal surface bears a low, ridge-like neural spine that is tallest along the caudal margin. As in LP4450, a neonate from the Early Cretaceous of Spain, the postzygapophyses bear large, dorsally directed epiphyses (Sanz et al., 1997).

The post-axial vertebrae are rectangular with large neural canals (slightly larger than the cranial articular surface), low and caudally displaced neural spines, and a ventral keel as in many enantiornithines (Chiappe and Walker, 2002). The following details are primarily based on the X-ray μ CT reconstruction of the first post-axial vertebra (Fig. 3). The neural canal is wide but low, vaulted dorsally with a nearly flat ventral surface. The ventral keel increases in depth caudally and its caudal portion extends slightly past the articular surface. The ventral surface is weakly concave between the ventrolateral margin and the ventral keel. The cranial articular surface is incipiently heterocoelous, mediolaterally elongated, and nearly three times as wide as dorsoventrally tall. The articular surface is cranially convex with a very weak central concavity (incipiently saddle-shaped). The entire surface is caudoventrally inclined, and the ventral margin (of the cranial articular surface) is slightly convex; low caudomedially directed ridges extend

from the ventrolateral corners of the cranial articular surface. The caudal articular surface is triangular, approximately as wide as tall; it appears to have a weak concavity centered on the articular surface. A similar, slight degree of heterocoely was reported in LP4450 and other enantiornithines (Sanz et al., 1997; Chiappe, 1996).

The reconstructed first post-axial vertebra also shows well-developed prezygapophyses (Fig. 3). The articular surfaces of these processes are large and asymmetrically oval, so that their caudal margins are narrower than their cranial margins. The length of the articular surface is craniocaudally longer than the pedicel of the prezygapophysis. The caudal margins of the articular surfaces are just rostral to the vertebral body. The articular surfaces are angled cranioventrally and medioventrally, so that the surfaces are tilted ventrally and toward each other. The ventral surfaces of the proximal end of the prezygapophysial pedicels bear a small, ventrally directed tubercle, probably the diapophysis. A short, longitudinal furrow excavates the lateral surfaces of the prezygapophyses. The postzygapophyses of the reconstructed first post-axial vertebra are similar in size to its prezygapophyses, but with shorter pedicels, so that the caudal margin of their articular facets is just distal to that of the vertebral body. The articular surfaces are crescent-shaped, with concave medial margins, and oriented caudoventrally. The dorsal surface of the postzygapophyses

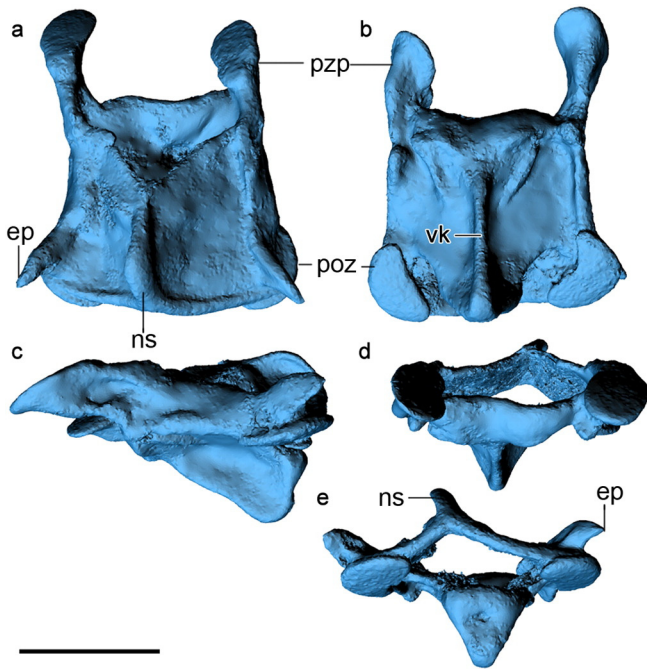


Fig. 3. X-ray μ CT reconstruction of the first post-axial vertebra: a, dorsal view; b, ventral view; c, lateral view; d, cranial view; e, caudal view. Anatomical abbreviations: ep, dorsal epicondyle process; ns, neural spine; poz, postzygapophysis; prz, prezygapophysis; vk, ventral keel. Scale bars equal 1 mm.

bears well-developed, hook-like epiphyses that end at the level of the caudal margin of the postzygapophysial articular surface. The first post-axial vertebra (number 3) is approximately subequal in length and width. However, the following three preserved vertebrae (fourth through sixth) are more elongate (longer than wide), and have longer prezygapophyses, a condition also reported in other enantiornithines (Chiappe and Walker, 2002). Delicate, sharply tapered costal ribs can also be discerned. Although unclear from the X-ray μ CT scans, they were most likely unfused to the vertebrae.

3.1.3. Partial wing

HPG-15-1 also preserves a partial distal wing; the distal ends of the right radius and ulna are in articulation with a poorly preserved hand (Fig. 4). As in all birds, the ulna is much more robust than the radius. The radiale and ulnare are both preserved; however the region of the wrist including the proximal carpometacarpus is unclear. The carpometacarpus appears weakly bowed so that the dorsal surface is convex, especially along the distal half; the minor metacarpal (III) appears nearly as robust as the major metacarpal (II) in dorsal view, but this may be due to poor preservation. In ventral view, it appears half the thickness. Also in ventral view, the minor metacarpal appears to project farther distally relative to the major metacarpal, as in all enantiornithines (Chiappe and Walker, 2002). It articulates with a reduced, rod-like phalanx that is slightly more than half the length of the first phalanx of the major digit and half the height and width. The alular digit is reduced, not reaching the distal end of the major metacarpal. A small claw is present, lacking distinct curvature (Fig. 4d). The first phalanx of the major digit is of the primitive non-avian morphology, as in other enantiornithines (as opposed to the craniocaudally expanded morphology shown in ornithuromorphs) (O'Connor et al., 2011). The penultimate phalanx of the major digit is shorter than the preceding phalanx as in most ornithothoracines. The ungual phalanx is similar in size and morphology to that of the alular digit.

3.1.4. Partial hind limbs

HPG-15-1 preserves the distal right tibiotarsus and complete right foot as well as part of the left pes (Fig. 6). Breaks in the bone reveal

that the metatarsals and phalanges are hollow. The absence of fusion between the tarsals indicates that the specimen is ontogenetically immature. The intermedium, forming the triangular ascending process, appears to be separate from the astragalus and calcaneum (Fig. S5)—this is known to be a stage in the skeletogenesis of the tibiotarsus of modern birds that is also recorded in young subadult or late-stage juvenile enantiornithines (Ossa-Fuentes et al., 2015). The ascending process is approximately twice the height of the tibiotarsal condyles. The medial condyle appears slightly wider than the lateral condyle, which is weakly excavated laterally. A single, free distal tarsal caps metatarsals III and IV. The proximal end of metatarsal II almost reaches the level of the cranial margin of the distal tarsal suggesting that another tarsal may be fused to metatarsal II. The metatarsals are completely unfused and their proximal ends are weakly expanded. Metatarsals II and III are subequal in thickness, whereas metatarsal IV is thinner and its distal trochlea is reduced to a single condyle, as in other enantiornithines (Chiappe and Walker, 2002). Metatarsal III appears to have been the longest, and metatarsals II and IV are subequal in length, although disarticulation and poor preservation of their trochleae leave the latter statement equivocal. Metatarsal IV has a flattened-oval cross-section with the long axis directed caudolateral-craniomedially so that the plantar surface is weakly excavated, as in some other enantiornithines (e.g., *Soroavisaurus*) (Chiappe, 1993). Metatarsal I articulates medially on metatarsal II, but is fully reversed so that the articular surface for the first phalanx of digit I is located perpendicular to the articular surface with metatarsal II, a morphology common in Early Cretaceous enantiornithines (e.g., bohaiornithids, pengornithids) (Zhou et al., 2008; Wang et al., 2014). The shaft of metatarsal I is mediolaterally thin and laterally concave so that it tightly articulates with metatarsal II. The shaft expands onto the plantar surface distally so that the distal end is much wider than the proximal portion of the shaft. The robust trochlear arm is perpendicular to the shaft and plantarly directed. This specimen suggests that a fully reversed hallux (anisodactyl foot) was broadly distributed among enantiornithines, a conclusion that is somewhat controversial based on the two-dimensional specimens from the Jehol, although a clearly reversed hallux is present in the Late Cretaceous *Neuquenornis* (Chiappe and Calvo, 1994), in which the J-shaped metatarsal I is extremely mediolaterally compressed, a condition somewhat different from that observed in Jehol enantiornithines and HPG-15-1.

The proximal phalanx of the hallux is incomplete on both sides. The claw of this digit is strongly recurved; nonetheless, it is shorter and broader than that of the other digits. All the ungual phalanges preserve ligamental grooves. The first phalanx of digit II is short and slightly more robust than the other phalanges in digits II–IV; the penultimate phalanx is the longest preserved phalanx, measuring 150% of the length of the preceding phalanx. The proximal end of the ungual phalanx of digit II is deeper than that of digit III, and it extends farther onto the dorsal surface of digit II's penultimate phalanx. Digit III is formed by three elongate phalanges of subequal length, followed by the longest claw in the foot (Figs. 6a, S5). The phalanges of this digit become increasingly more delicate toward the distal end of the toe. Digit IV consists of four short subequal phalanges followed by the smallest claw in the foot. The penultimate phalanx is slightly longer and more delicate than the preceding phalanges. Visible in the third phalanx of this digit, the lateral condyle of the distal trochlea appears to be more strongly plantarly projected. Digit III is by far the longest followed by digit IV, and then digit II, so that the foot is asymmetrical. Pits for the collateral ligaments are visible on the phalanges but are not observable on the medial and lateral surfaces of metatarsal III. The proportions of the pedal digits (being long with distally elongated phalanges in digits II and IV), suggest an arboreal lifestyle, as it has been hypothesized for most other enantiornithines (O'Connor, 2012).

Although lacking sufficient contrast to show up in osteological examinations using X-ray μ CT, the proximal right femur appears to be preserved (Fig. 1a, c), observable with high intensity transmitted light and

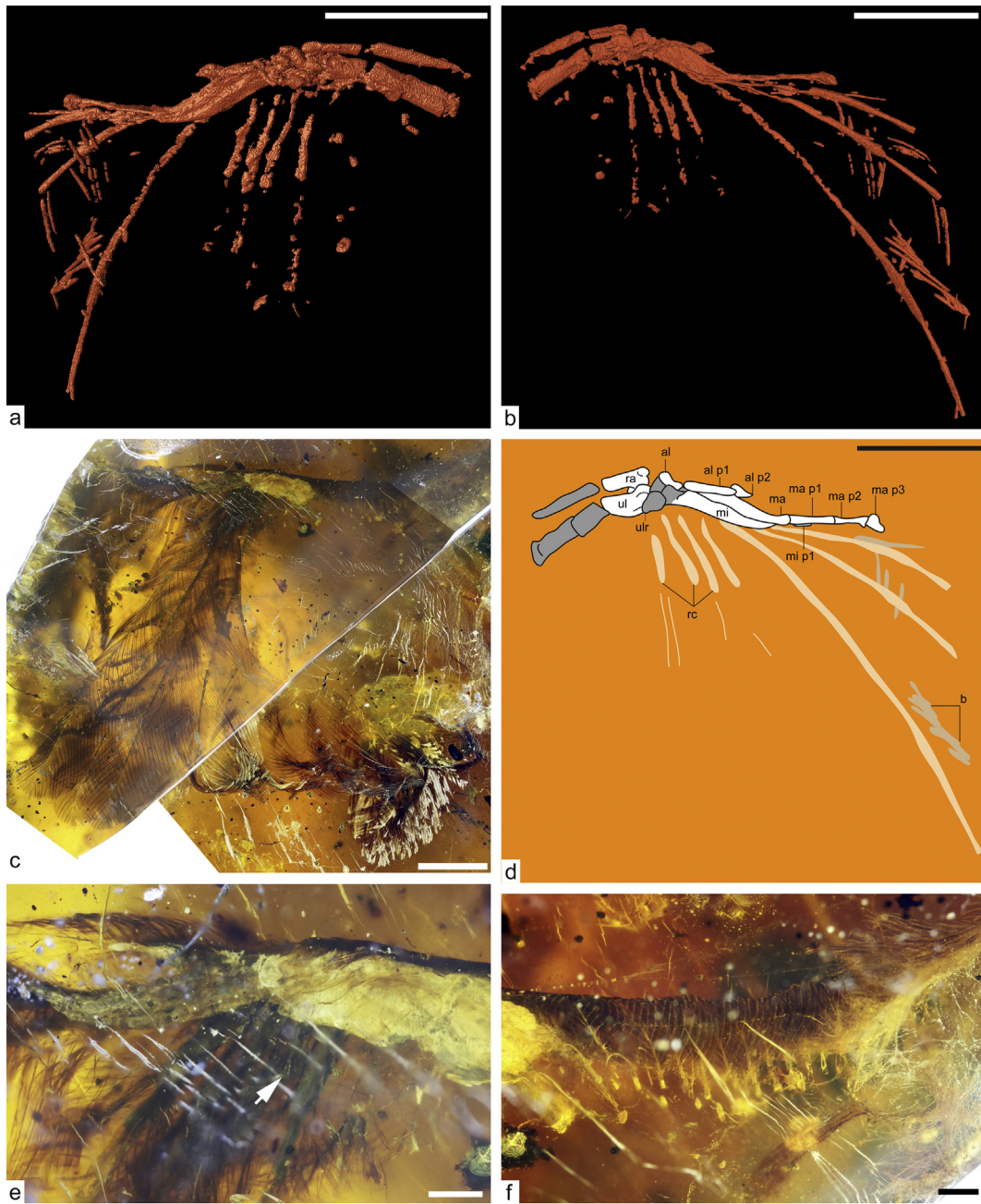


Fig. 4. Details of wings and plumage in HPG-15-1. a, b, X-ray μ CT reconstruction of preserved wing bones and feather bases, plus partial representation of barb rami, in ventral and dorsal view, respectively; c, distribution and weathering of feathers, utilizing composite of three separate images; d, interpretative drawing of the wing in dorsal view based on X-ray μ CT reconstructions (panel b); e, bases of primary remiges with calamus (arrow), naked surface of manus, alula, and large mass of milky amber adjacent to broken ends of radius and ulna; f, weathering surface exposing underside of coverts on propatagium and their follicles, plus broken end of ulna (arrow), and loose contours from humeral or dorsal tract (right edge of image). Scale bars equal 5 mm (a–c), 1 mm (e, f). Abbreviation scheme: al (alular metacarpal); b (barbs); ma (major metacarpal, III); mi (minor metacarpal, II); p (manual phalanx) number in Arabic numerals; ra (radius); rc (rachis); ul (ulna); ulr (ulnare).

reflected light. Although poorly preserved, the cranio-lateral margin appears to be angled ventrally as in many enantiornithines (Chiappe and Walker, 2002). The orientation of the femur indicates it is not preserved in its natural position.

3.2. Integumentary structures

In general, the skeletal material within HPG-15-1 is surrounded by feathers and the translucent remains of integument that represent most of the right side of the body. Although the feathers are clearly visible through a combination of incident, transmitted, and high-angle lighting, the surface of the skin itself can be quite difficult to discern.

Fortunately, the presence of feather insertions provides an opportunity to map out the extent and characteristics of the preserved integument and its structures (Fig. 1c).

3.2.1. Head and neck

The articulated skull and series of cervical vertebrae bear plumage in dense fields both ventrally and dorsally (the cervical tracts), separated by a lateral cervical apterium (Fig. 2c–d). The individual feathers in each tract are dark brown in color, and appear to consist of tufts of four or more barbs that extend less than 1 mm in length from their shared base (Fig. 2f). Unlike neoptile feathers or natal down in modern birds, the barbs among the cervical plumage in HPG-15-1 are bristle-

like, with no clear indication of barbules or a central shaft. There is also no visible sign of sheathing or a previous generation of feathers stemming from these follicles. The simplest interpretation of the visible structures is that they represent a field of newly erupted contour feather apices. If this is the case, we are unable to see the short sheathes that hold the barbules together basally, due to translucency; and the barbules that are exposed appear solid because of dark, diffuse pigmentation and a lack of well-defined segmentation (*i.e.*, stylet barbules; Lucas and Stettenheim, 1972). Alternatively, these feathers may be the protruding tips of bristles or reduced contour feathers (*i.e.*, naked barbules), similar to the second-generation feathers found on the necks of extant megapodes such as the brush-turkey (*Alectura lathami*) (Wong, 1999).

The external opening of the ear is elliptical in shape and its outline is visible on the right side of the head (Figs. 1c, 2c, d). This region is surrounded by a narrow auricular tract of feathers nearly identical to the cervical feathers, but the tufts surrounding the ear contain fewer barbules, and are oriented so that their apices all face inward, toward the opening of the ear. The cervical tract connects seamlessly with a broader occipital tract. However, feathers within the coronal tract appear to be restricted largely to the dorsal surface of the head, with no indication of a dorsal crest. Skin is preserved as a translucent film in unfeathered regions of both the head and neck. These apteria include most of the postauricular, auricular (anterior to the external ear opening), malar, and submalar areas. Plumulaceous feathers are absent from the apteria, and they are also absent from the spaces between feathers.

The anterior and ventral regions of the head are difficult to observe due to the thickness of the overlying amber in this region, coupled with the density of clay-filled bubbles and carbonized plant fragments in the surrounding amber. However, careful lighting reveals the outline of the eye and provides a limited view of the anterior portion of the dentary. The eye is large and bulbous, projecting laterally from the surface of the head (Fig. 2c, d). The view is not clear enough to be certain, but it seems the eyelid may be closed, forming a slit that is situated within the ventral one-third of the ocular height. The rostral margin of the dentary displays the same jagged edge that was observed in the X-ray μ CT data (Section 3.1.1) when viewed with strong incident light (Fig. 2c, e). However, this does not provide a clear indication of teeth. The dentary appears to be darkly pigmented, suggesting that a horny beak may have been present.

3.2.2. Partial wing

The right wing in HPG-15-1 is incomplete and shows obvious signs of exposure and weathering (Fig. 4). Both skeletal material and integumentary structures from the wing's apex are well-preserved, but the basal parts of the wing have been truncated between resin flows, reducing these regions to partially preserved feathers and small flaps of skin. The dorsal surface of the wing has been weathered strongly, creating a situation in which the perimeter of the wing is well-represented, but the central and apical parts of the wing are largely missing (Figs. 1c, 4). Consequently, the plumage preserved consists of fragments of some of the primaries, and alula feathers, some of the secondaries and coverts, and traces of contours from the wing base.

There are eight primaries preserved in HPG-15-1. For the most part, these feathers are deeply buried within the amber mass, and have been truncated apically (Fig. 4). The primaries are missing their apices because they have been swept anterad by flows within the surrounding resin and cross the plane of surface exposure that truncated the wing. The apical primaries are asymmetrical, and they do not differ dramatically from the basal primaries in terms of preserved color patterns or rachis dimensions, but few other features of these feathers can be observed—even their exact number remains unclear. Primaries I–IV are preserved completely, and are better exposed than the apical primaries. These complete feathers reach lengths of 27 mm and are strongly asymmetrical. The rachises appear to be subcylindrical in cross-section and pale throughout most of their lengths. They do not have the medial longitudinal stripe that has been observed among the

remiges of the basal enantiornithine *Eopengornis* (Wang et al., 2014). Each rachis is expanded basally, and has been preserved with a dark grey color that appears nearly black along the margins (Fig. 4e). This dark region seems to represent the calamus (Fig. 4e), and some of the feathers display insertion points for downy feathers that overlie this region (Fig. S3a). There are no signs of afterfeathers or umbilical barbules on the primaries. Barbules with pennaceous barbules are present along the length of each rachis, extending basally to within less than 2 mm of the contact with the metacarpals. Barb rami are narrow and deep (ovoid in section), and appear to have been somewhat flexible—some barbules have been distorted into sinuous sheets due to movement within the encapsulating resin, but the barbules have not detached from one another. Both proximal and distal barbules are blade-shaped throughout most of their lengths: approximately seven basal cells can be distinguished based on faint patterns within the pigmentation, and these are followed by a poorly differentiated pennulum. Details of the hooklets on the barbules are not visible due to the thickness of overlying amber. However, each of the complete primaries is preserved with visible color patterning that consists of a walnut brown color interrupted by a pale feather apex and two pale transverse bands in the distal half of the feather (Figs. 4c, 5a).

Secondary feathers 1–9 are preserved as fragments in HPG-15-1, with two feather bases, and nine apices visible. The central core and apical margin of each secondary feather is preserved with a pale brown color, while the lateral margins of each vane are preserved with a much darker walnut brown color. There are numerous spots within the secondary feathers where the feather has withdrawn from the surrounding amber, leaving a reflective or milky surface (Figs. 4c; 5c, d). This taphonomic feature is more common within the secondaries than the primaries, and may be related to flexion or a byproduct of feather oils. The secondaries display greater apical flexibility than the primaries, with many barbules curving back toward the feather base or moving relative to their neighbors (clumping or splaying), due to anterad resin flow across the wing. Barbules on the secondaries possess the same general appearance as those on the primaries, but their truncation at the line of exposure provides a clearer view of structure and pigmentation in a few places (Fig. 5). Here too, there is little visible distinction between the base and pennulum of each barbule, and there appear to be approximately seven basal cells.

Only one of the alula feathers is preserved and clearly visible within the wing. It is asymmetrical and comes to an acute point, and barbules on its trailing edge are significantly paler than those on the leading edge of the feather. There may be additional alular feathers in more posterior positions, but these are not visible due to overlap, or perhaps due to pale plumage in this wing region (as in other specimens from this deposit: Xing et al., 2016a). A veil of milky amber that is likely related to the release of decay products extends from the base of the alula, obscuring most of the radius and ulna. Protruding through this veil is a short, sparse series of neoptile feathers that are pale in color (*i.e.*, pale brown). The ventral surface of the manus lacks plumage, and the exposed skin has a mottled grey, tan, and black surface that may be related to partial carbonization or saponification of the soft tissues, or to a thin layer of milky amber produced by decay products or moisture interacting with the surrounding resin (Martínez-Delclòs et al., 2004).

Covert feathers from the upper margin of the propatagium are visible along the leading edge of the wing (Figs. 4f, S3a). They are viewed through the ventral surface of the wing because most of the wing posterior to these feathers has been obliterated by exposure along a drying line in the amber. The coverts point more anterad than adapically. Their pigmentation appears uniform and diffuse throughout the barbules and is slightly darker than the walnut brown color preserved in the secondary feather apices, but the rachises and barb rami within the coverts are pale or white in color, and the feathers become progressively paler near their bases. Where the coverts meet the body plumage from the shoulder region (either humeral or dorsal tract), there is a pronounced change in feather morphology (Fig. 4f). The dorsal body contour feathers have elongate and flexible barbules in an open

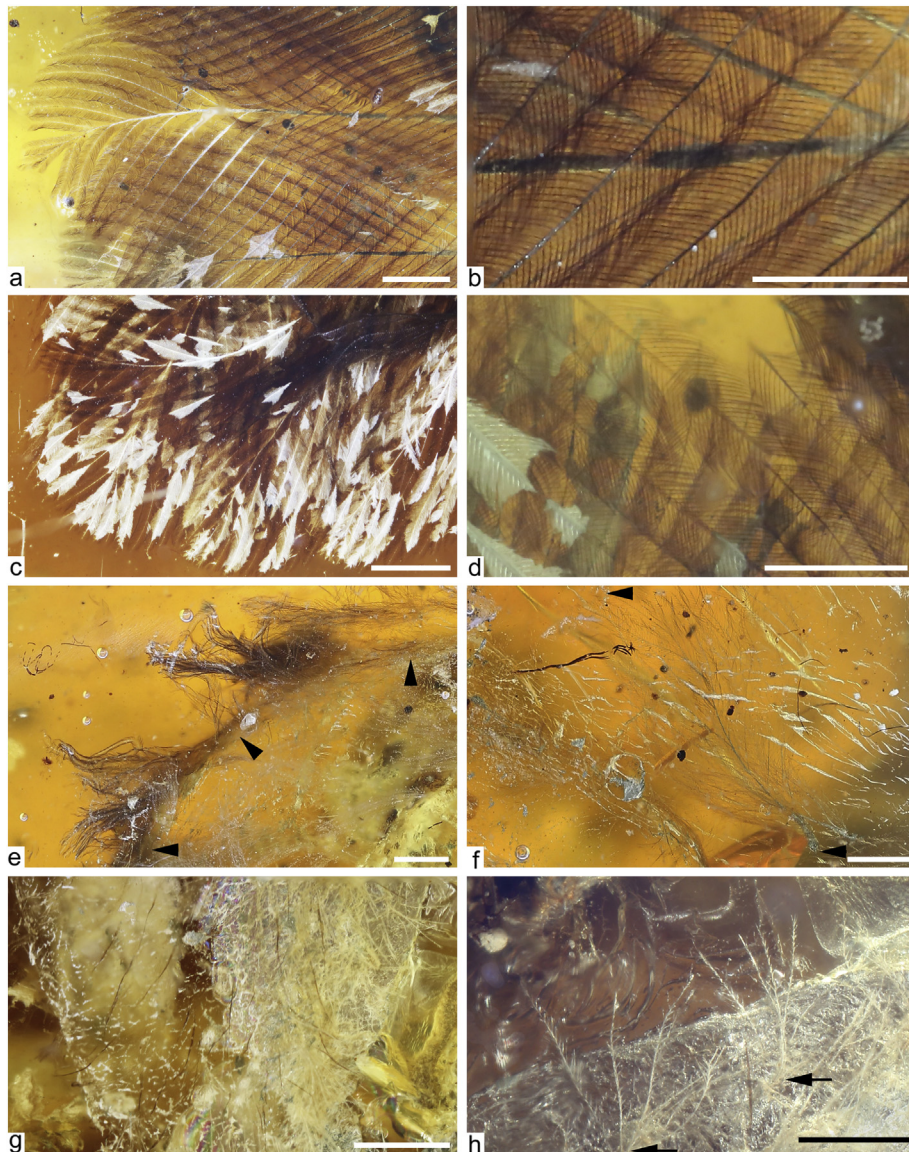


Fig. 5. Microstructure and pigmentation of feathers on wing and body of HPG-15-1. a, primary remiges with transverse pale band near center of image; b, structure and pigment distribution in barbs and barbules near lower right corner of (a); c, secondary remiges with darker brown colouration, and pale taphonomic artifacts; d, structure and pigment distribution in barbs and barbules of secondary feathers, and clearer view of separation layer causing artifacts in (c); e, contour feathers in pelvic tract, with arrowheads marking dorsal edge of preserved skin; f, contour feathers with plumulaceous bases, in lateral pectoral tract; with arrowheads marking base and apex of single pale feather; g, mixture of pale 'neoptile' feathers and brown filaments within the crural tract; h, magnified view of 'neoptile' feathers near upper right margin of (g), rotated counterclockwise, and with arrows indicating insertion points for feathers. Scale bars equal 1 mm in (a, c, e–g), 0.5 mm in (b, d, h). (For interpretation of the references to color in this figure legend, the reader is referred to the web version of this article.)

arrangement. Body contours in the surface layer of the plumage have barbs with medium brown margins contrasting against markedly paler barb rami and basal barbule sections. There is no indication of a rachis longer than the barbs among these feathers. Contours composing the understory layer of the body plumage are pale or white, and may conceal plumulaceous feathers or plumulaceous bases within their dense, tangled mass. Unfortunately, the available exposure and lack of color contrast does not provide a clear view of this understory material. The body contours that are exposed from the limited exposure of the pelvic tract and dorsal caudal tract (Figs. 1c, 5e, posterior to the wing) appear to be nearly identical to those of the shoulder region, albeit with less density in posterior regions. Few feathers from the lateral pectoral tract are visible. These pectoral feathers are elongate, pale or white contours, and have weakly developed rachises (Figs. 1c, 5f). They exhibit an open pennaceous overall structure and appear to consist of plumulaceous barbs basally, and pennaceous barbs with blade-shaped barbules apically.

A single flight feather apex is preserved between the ankle and tail of HPG-15-1 (Fig. 1). This appears to be a secondary feather that may have detached from the surface of the preserved right wing, or alternatively, may represent a fragment of the left wing within the piece of amber. Based on its position and orientation, and the anterad deflection of secondaries on the right wing, the latter explanation is the most parsimonious. There may be part of a second feather hidden behind the secondary, but its details are unclear due to the extent of overlap.

3.2.3. Partial hind limbs

In addition to osteological features, the hind limbs preserve feathers and traces of skin. Thick-skinned regions, such as the foot, are easily observed, but the remainder of the leg is only represented by a faint outline of translucent skin and pale, sparse plumage.

Plumage within the femoral and crural tracts consists of neoptile feathers with a short or absent rachis, and barbs that bear blade-like pennaceous barbules (Fig. 5g, h). These neoptile feathers are nearly

transparent, suggesting that they were pale or white. Interspersed among the neoptile plumage are isolated bristle-like filaments (IBFs) of a medium brown color (Fig. 5g) that are less than 1 mm long. These IBFs are widely spaced and occur in isolation (stemming from separate follicles), with greater density in the distal portion of the crural tract. Their deflections within the resin, combined with variations in their thickness (ranging from ~21 μm to 5 μm or less in a single filament), suggest that the IBFs are flattened in one dimension and twisted slightly throughout their lengths. No trace of a crural flag is present on the leg, and the femoral tract bears the same widely spaced neoptile feathers as the crural tract, but lacks the additional IBFs found in the crural tract.

The skin beneath the crural tract is thin and smooth, but the metatarsal tract bears pronounced, oblong scutellae that continue across most of the digit surfaces. Additional linear features traverse the metatarsal tract; these are not integumentary structures, but a series of taphonomic cracks within the tissue that run subparallel to one another (Fig. S3b). The dorsal margin of each digit bears a single line of narrow scutes that are difficult to distinguish from their neighboring oblong scutellae due to their similar size and the lateral view that is available. Reticulae are more circular in outline and much finer on the plantar surface of the tarsus, becoming minute between digital pads. The digital pads are prominent enough to be clearly visible in lateral view, and

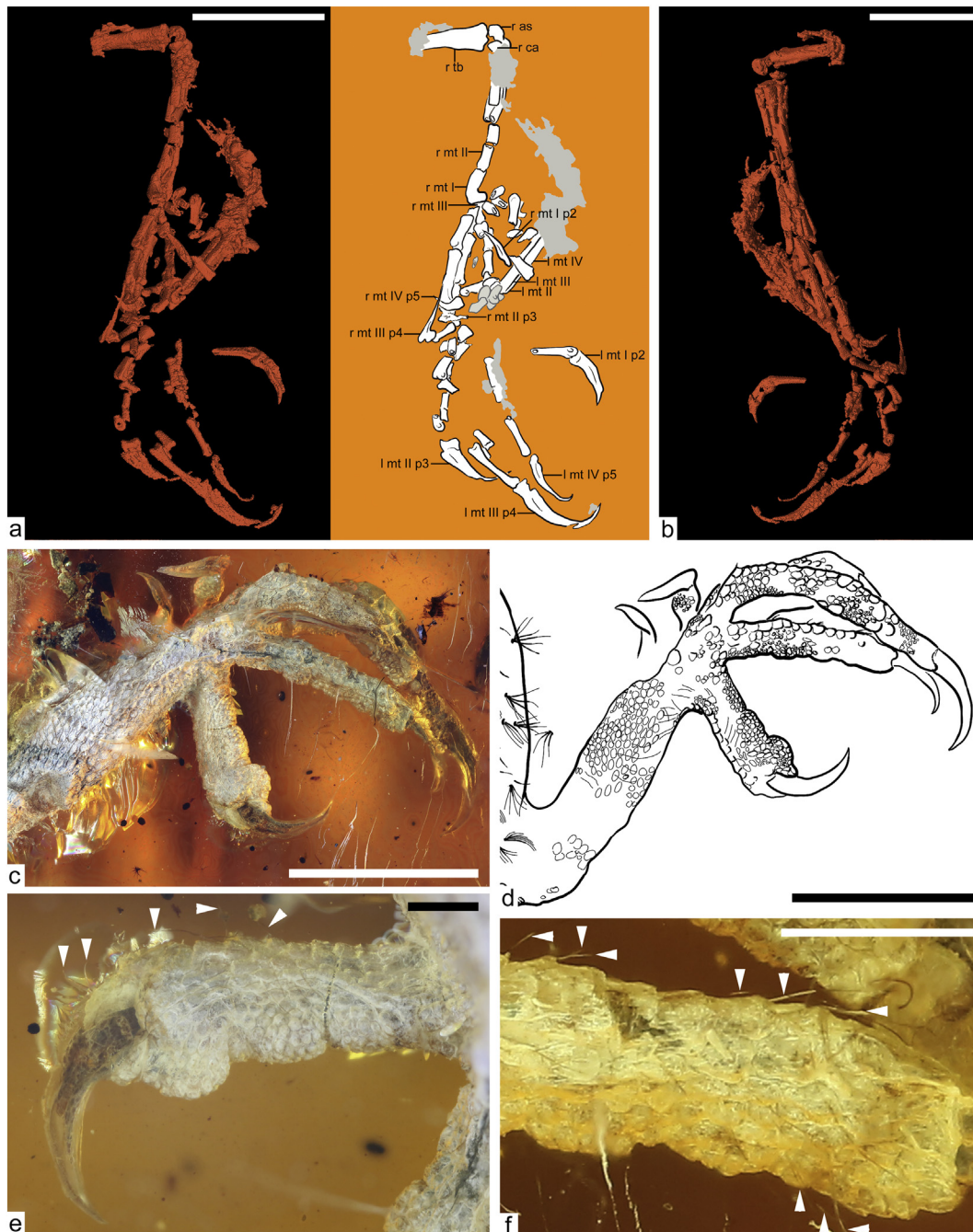


Fig. 6. Details of the feet of HPG-15-1. a, X-ray μCT reconstruction and interpretative drawing of the preserved hindlimb bones with the right tarsometatarsus in medioplantar view; b, X-ray μCT reconstruction of the preserved hindlimb bones with right in dorsal view; c, d, right foot integumentary details and illustration of scutes, scutellae, reticulae, and taphonomic cracking of skin in foot, with feather barbs from crural neoptile plumage indicated; e, f, higher magnification views of skin surface and bristles (near arrowheads) on digits I and II. Scale bars equal 5 mm (a–d) and 1 mm (e, f). Abbreviation scheme: r (right) or l (left) as prefix; as (astragalus); ca (calcaneum); dt (distal tarsal); mt (metatarsal) number in Roman numerals; p (pedal phalanx) number in Arabic numerals; tb (tibiotarsus).

the apical digital pad on digit I is greatly expanded. The preserved claws are described in Section 3.1.4. The heel pad is prominent (Figs. 6c, S3b) but its details are obscured by a large bubble that emanates from the broken end of the left shank, and reflective cracks that expand outward from the right metatarsus further impair observation of its margins and plumage. The digits bear filaments that somewhat resemble those found within the crural tract, except the filaments on the digits originate from the distal part of scutellae and most are directed distally (Fig. 6c–f). These scutellae scale filaments (SSFs) are present sporadically on the dorsal surface of the digits, and to a lesser degree, on the lateral surface of the digits. In some instances, the apical filaments are directed toward the plantar surface; however, these filaments still appear to stem from scutellae as opposed to the reticulae.

3.2.4. Partial tail

Although there is no visible trace of skeletal material posterior to the femur fragment mentioned in Section 3.1.4, the outline of the tail is clearly visible through a combination of translucent skin surface preservation, constrained decay products (milky amber), and plumage stemming from the integument (Figs. 1, 7a, b). The outline created by this combination of features is straight and gently tapering, with an overall length of approximately 9.5 mm excluding plumage. The apparent broadening of the tail that occurs caudally is likely a taphonomic artifact caused by one of the larger rectrices folding back on the dorsal surface of the tail due to resin flows.

The tail tissue contains three distinct feather types. The lateral margins bear a row of unpigmented (pale or white) feathers that are somewhat consistent with neoptile plumage in modern birds. The 'neoptile' feathers have four to six barbs that are approximately 1 mm long, and stem from a diminutive rachis or share a common base. These barbs are nearly transparent (likely white in life), and bear pennaceous barbules that are elongate and blade-shaped. Barbule lengths can be as high as 150 μm basally, and gradually diminish toward the apex of each barb. In addition to the neoptile feathers, the apical portion of the tail also bears darkly pigmented IBFs (Fig. 7b). The IBFs are arranged singly (stemming from separate follicles) along the lateral and dorsal surfaces of the tail, with increasing density caudally. The visible IBFs have maximum widths that range from 15 to 27 μm near their midlengths, with the longest visible IBF reaching 1.06 mm in length.

Dimensions among the IBFs are difficult to assess, because they are flexible and appear to be slightly flattened in width.

The tip of the tail clearly preserves the remains of a single large sheathed rectrix (Fig. 7b). The caudal thickening of the tail appears to be a product of a second large rectrix folding back on the surface of the tail, but details of the structure are clouded by milky amber. The apical diameter of the better-preserved rachis exceeds that of the remiges (170 μm vs 120 μm). The only feathers in a bird that are larger than the remiges are rectrices modified for ornamentation. Although the soft tissue of the tail is clearly incomplete, the apparent presence of a pair of enlarged rectrices is consistent with the presence of paired rachis dominated tail feathers (rachis enlarged compared to normal flight feathers) observed in compression fossils of numerous enantiornithines including juveniles (Zheng et al., 2012; de Souza Carvalho et al., 2015). This is further supported by the absence of gradation in the feathers leading into the enlarged rectrix. The well-preserved rectrix has a basal insertion that is an order of magnitude wider than most of the other feathers on the tail (~170 μm), and it extends more than 2.3 mm from the apex of the skin outline. The feather sheath is cylindrical throughout most of its length; however, there are gaps in the visible length of the preserved sheath that may be an artifact of preservation (variation in opacity due to decay products or oils interacting with the surrounding resin, or the sheath disintegrating). Alternatively, these gaps may indicate that the sheath is preserved in the process of opening to release the second-generation feather at this site. The sheath tapers to an acute point followed by a somewhat cylindrical expansion, which is presumably the calamus from the first-generation feather (Fig. 7b). A short cluster of barbs extends from the calamus, but their exact characteristics are obscured by the extent to which they overlap, and their near-transparency. These barbs bear barbules, but it is unclear whether the barbules are plumulaceous or more pennaceous in form.

3.3. Taxonomic assessment

The J-shaped morphology of metatarsal I, the presence of a metatarsal IV that is thinner than metatarsals II and III, and the reduced and single-condyle trochlea of this metatarsal support the identification of HPG-15-1 to the Enantiornithes (Chiappe and Walker, 2002). This is further supported by the absence of fusion between the tarsals and metatarsals (which are typically fused in ornithuromorph specimens), the

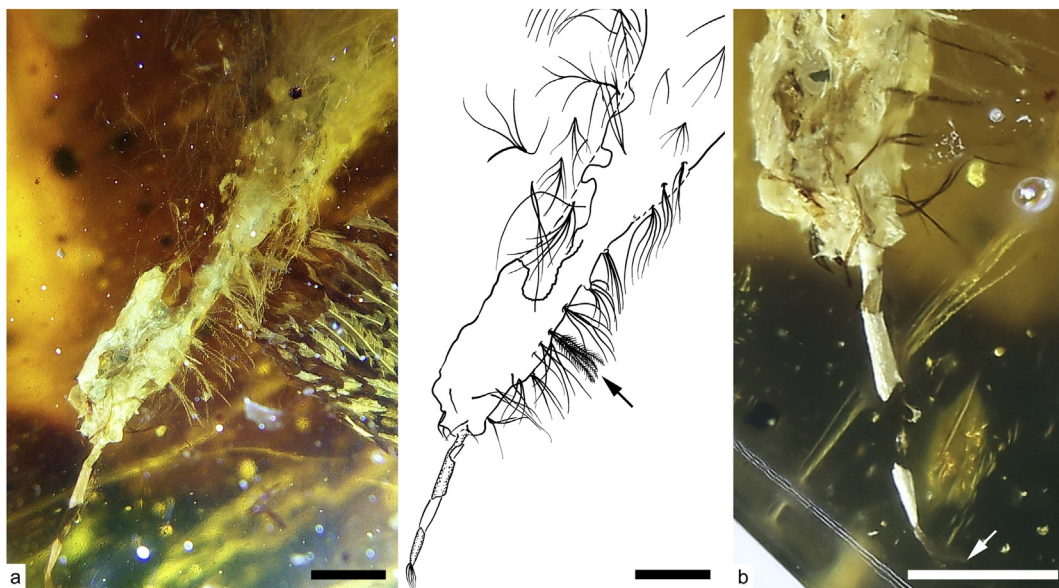


Fig. 7. Details of the tail of HPG-15-1. a, overview of plumage on tail, with matching illustration of feather distributions (barbules omitted on all but one 'neoptile' feather situated near arrow); b, higher magnification view of medial rectrix sheath and first-generation feather (arrow), plus brown filaments interspersed with neoptile feathers. Scale bars equal 1 mm. (For interpretation of the references to color in this figure legend, the reader is referred to the web version of this article.)

proportions of the pedal phalanges (distally more elongate), and the presence of large and recurved pedal unguals (O'Connor, 2012). Although fusion is affected by ontogeny (and it is not unique to Enantiornithes among non-ornithuromorph birds) and the proportions of the pedal phalanges relate to ecology, currently among Cretaceous birds only enantiornithine specimens display this suite of characters. The presence of cervical vertebrae that are only cranially heterocoelous is also characteristic of enantiornithines (Chiappe and Walker, 2002). The normal shape of the first phalanx of the major manual digit (expanded in ornithuromorphs), and the fact that the penultimate phalanx of this digit is shorter than the proximal phalanx (longer in more primitive birds), also indicate that HPG-15-1 belongs to the Enantiornithes. A minor metacarpal that projects farther than the major metacarpal is an enantiornithine synapomorphy (Chiappe and Walker, 2002); however, this feature is somewhat equivocal in this specimen. The precocial wing plumage consisting of fully developed remiges present in HPG-15-1 is also a feature that, among Mesozoic birds, is so far only recognized within this group (Chiappe et al., 2007; de Souza Carvalho et al., 2015; Xing et al., 2016a). Among Cretaceous birds, an enlarged pair of rectrices is only observed in enantiornithines and confuciusornithiforms.

3.4. Ontogenetic assessment

The absence of fusion between the intermedium and astragalus/calcaneum, and between these elements and the tibia, and the absence of fusion between the larger distal tarsal and the proximal metatarsals, all indicate that this specimen is immature, consistent with its very small size. These elements fuse in adult enantiornithines (Hu and O'Connor, 2016). Apparent fusion in the mandible may be taphonomic or due to the low scan resolution, as the dentary and postdentary bones are not fused in other known embryonic and juvenile enantiornithines (Elzanowski, 1981).

The feathers associated with the head, wing fragment, and hind limbs in HPG-15-1 are consistent with the precocial or superprecocial plumage found in both compression fossils (Chiappe et al., 2007) and amber-entombed fossils (Xing et al., 2016a) attributed to the Enantiornithes. The presence of neoptile feathers and extensive skin areas with low-density plumage both point toward an even earlier ontogenetic stage than previous specimens discovered in Burmese amber (Xing et al., 2016a). However, the unfurled and dried morphology of the remiges, presence of feathers in possibly their second generation (e.g., cervical tract) and others already in the process of molting (e.g., the sheathed rectrices), and the presence of a conspicuous eye slit indicate that HPG-15-1 was a hatchling as opposed to a late stage embryo.

4. Discussion

4.1. Enantiornithine development

The individual HPG-15-1 is considered a juvenile enantiornithine (see Results Sections 3.3 and 3.4). Measurements of the skull, wing, and foot in HPG-15-1 were compared to three other nearly complete juvenile enantiornithine specimens (UFRJ-DV-031Av from Brazil, and STM34-7 and IVPP V15664 from the Jehol) and a late-stage embryo (IVPP V14238 from the Jehol) (de Souza Carvalho et al., 2015; Zheng et al., 2012; Zhou and Zhang, 2004). The proportions of the skull, wing and foot are consistent with the taphonomic assessment that these elements all belong to a single individual. The proportions in the new specimen are more similar to those in the late-stage embryo from China (IVPP V14328) than to those of juvenile specimens (skull proportionately larger, hand proportionately smaller; see Supplementary Table S1), strongly suggesting HPG-15-1 represents a neonate, consistent with its very small size (smaller even than IVPP V14328). The embryo preserves traces interpreted as rectrices that suggested at least some enantiornithines hatched volant (Zhou and Zhang, 2004). The

plumage preserved in HPG-15-1 contributes to mounting evidence that enantiornithine hatchlings were volant and highly precocial (Starck and Riecklefs, 1998); Chinsamy and Elzanowski, 2001; Zhou and Zhang, 2004; Chiappe et al., 2007; Zheng et al., 2012; Mayr, 2016).

Living birds have a wide spectrum of developmental patterns: as a result, the maturation of neonates varies between species, forming an altricial to precocial gradient that has traditionally been defined by combinations of morphological and behavioral characteristics (Starck and Riecklefs, 1998). On one end of the spectrum there are helpless altricial chicks born blind and naked, and on the other lies the superprecocial chicks of the Megapodidae (Galliformes), independent and capable of short bursts of flight within 24 h of hatching (Starck, 1993; Starck and Riecklefs, 1998). In contrast to the Neornithes, the enantiornithine spectrum appears more limited with all available evidence indicating chicks were highly precocial. This is most likely due to physiological constraints on egg size due to the distally contacting pubes present in non-ornithurine birds (Kaiser and Dyke, 2010; Mayr, 2016). This limited developmental variability probably would also have excluded enantiornithines from breeding in some of the extreme environments utilized by living birds, where chicks would otherwise perish without large amounts of parental care. These limitations may further explain the absence of enantiornithines with aquatic adaptations. Although the degree of post-natal parental care is unknown, enantiornithines are both highly precocial and arboreal, a combination not observed among living birds, in which arboreal birds have altricial chicks (Riecklefs, 1973) and the superprecocial megapodes are primarily terrestrial and poor fliers. This means that enantiornithines do not fit within the developmental morphospace of modern birds, also evidenced by the relatively early timing of reproductive maturity, lower growth rates and protracted growth (Chinsamy et al., 1995; O'Connor et al., 2014). Slow post-natal growth results in a protracted period of vulnerability, which is reflected in the Enantiornithes by the large number of juveniles found in the fossil record (Chiappe et al., 2007; Zheng et al., 2012; de Souza Carvalho et al., 2015), whereas young juveniles of other Cretaceous bird lineages are unknown. Similarly, thus far, only young juvenile material has been collected from Burmese amber.

4.2. Plumage and integumentary structure implications

The feathers surrounding HPG-15-1 provide a more comprehensive representation of plumage in a juvenile enantiornithine than any previous specimen, but they pose as many questions as they answer. Unusual feather morphotypes, such as the IBFs observed on the leg and tail, suggest that small numbers of protofeathers may have been retained in taxa closely related to ornithuromorphs. However, these may only be retained in early plumages and lost in adults. Meanwhile, some of the neoptile plumage is an imperfect match for that found in modern birds. Among these insights, the feathers themselves shed some light on the developmental stage of the animal at the time of preservation.

The sparse coverage of neoptile feathers and down found on the legs, ventral trunk regions, and along the tail of HPG-15-1 suggests that this individual had only recently hatched. Feathers were already starting to erupt from the follicles on the neck and head, or to replace neoptile plumage within the tail, but this process is in its early stages. If we examine modern chickens as an example of molt timing (Lucas and Stettenheim, 1972), the medial rectrices begin to transition into second-generation feathers two days after hatching, while rectrices in lateral positions take progressively longer to develop (17–25 days until all rectrices have begun the transition); the dorsal cervical tract begins to receive secondary feathers 10–18 days after hatching; and the legs tend to enter the second molt slightly later (12–133 days after hatching for the femoral tract, and 20–84 days for the crural tract). Admittedly, this is an imperfect modern analogue: mature wing plumage is known in enantiornithine embryos (Zhou and Zhang, 2004), while a chicken may not possess a complete set of mature second generation primaries until 82–100 days after

hatching (Lucas and Stettenheim, 1972). This gets further complicated by the fact that enantiornithine ontogeny was unlike that of any living bird and was probably associated with differences in molt morphology and timing (as already evidenced by differences in appearance of ornamental feathers; Zheng et al., 2012). Nonetheless, the body regions in HPG-15-1 excluding the wings seem to follow the same general molt pattern as seen in modern birds, and the developmental point preserved in HPG-15-1 would fall within the first days or weeks of development in this context. Modern megapodes, such as the brush-turkey, only exhibit neoptile plumage in the tail region for the first week of life (Wong, 1999). If molting proceeded at an accelerated rate in all body regions of Enantiornithes, the new specimen may represent an individual that is in the first few days or first week of life. If the incoming rectrices are interpreted as ornaments, the presence of these feathers in juveniles would represent a distinct departure from neornithines in which sexually dimorphic ornamental feathers do not typically appear until reproductive maturity is achieved, which occurs after the bird is skeletally mature (Gill, 2007; Zheng et al., 2012). Although known to be present in juveniles, the presence of erupting rectrices in this very young individual suggests that these feathers were not present upon hatching but appeared in the first molt. The lack of dense insulative feathers on the legs and belly also stands in contrast to the dense arrangement of contour feathers found in modern superprecocial birds, such as the brush-turkey (Wong, 1999). The sparsely feathered regions include IBFs, which resemble primitive holdovers from early stages in feather evolution. In contrast, juvenile specimens, often preserving paired rachis-dominated rectrices, have well-developed body feathers (de Souza Carvalho et al., 2015; Zheng et al., 2012). This suggests that enantiornithines were born with sparse body feathers including very primitive morphologies, which were rapidly replaced with a mature plumage. Alternatively, these differences reflect a diversity of developmental strategies among different enantiornithine clades.

Despite the early developmental stage observed in this specimen, most of the 'neoptile' feathers observed are more morphologically consistent with contour feathers than with modern down. There are very few places within the plumage where anything resembling a modern plumulaceous barbule can be found, and most of these instances are only referred to as plumulaceous herein because the barbules appear elongate and filamentous, not because they contain well-developed nodes and internodes. Most body regions outside of the wing bear plumage that is more contour-like in appearance, with pennaceous barbules. Within the femoral, crural, and caudal tracts, the pennaceous barbules are longer toward the base of each barb, but they are not replaced by plumulaceous barbules in these positions, even in feathers with a short or reduced rachis. It is unclear whether the feathers with reduced pennaceous barbules and an open-vented structure are fulfilling the same functions as natal down and neoptile feathers (*sensu* Foth, 2011) do in modern birds; whether natal down (if it ever existed) has already been shed from the follicles involved; or if Enantiornithes underwent a different pattern of molts than their living relatives. The latter is becoming increasingly likely as differences between enantiornithine and neornithine plumage are elucidated through fossils such as HPG-15-1. Ultimately, we will need an extended growth series, or at least some specimens that show clearer evidence of the molting patterns and processes to address these questions. In the meantime, the presence of 'neoptile' feathers alongside medial rectrices undergoing their first molt strongly suggests that this unusual morphotype is representative of the first generation of feathers in this specimen.

Generally, the pterylosis and ptilosis observed in HPG-15-1 match well with that of modern birds (Lucas and Stettenheim, 1972). However, unusual morphotypes are present. The morphology of the SSFs largely match predictions made by Dhouailly (2009), based on developmental manipulation. The visible plumage erupts from the distal portions of scutes and scutellae, and not from the reticulae.

Conversely, the IBFs within the crural tract and on the tail bear greater similarity to the Stage I protofeathers suggested by evolutionary developmental model of Prum (1999). This suggests that the plumage of HPG-15-1 included highly reduced forms of Stage V feathers together with Stage I equivalent feathers (in the model of Prum, 1999). The function of these bristle structures (IBFs and SSFs) is unclear. Given that HPG-15-1 is a very early stage juvenile specimen, the production of reduced bristles across numerous body regions seems unlikely. In modern birds, bristles typically serve specialized tactile functions and often retain some traces of barb branching or the structure of the rachis (Lucas and Stettenheim, 1972). It is unlikely that diminutive forms of bristle feathers would appear among the neoptile plumage, and with dimensions that are more comparable to a barb ramus than to a rachis. Until we can observe these filaments in greater detail and preferably in cross-section, their categorization will remain open to debate. However, the balance of evidence currently available suggests that IBFs and SSFs are most likely an evolutionary holdover as opposed to derived structures. A brief examination of hatchlings within the RSM collection suggests that at least some extant birds have bristles or filaments with similar gross morphology stemming from their scutes (Fig. S4). However, a much more extensive survey of modern birds and comparisons at more than just a superficial level (*i.e.*, detailed sectioning studies of both modern and fossil counterparts) are necessary to assess the true extent of this similarity. If the early ontogenetic stages of extant birds retain traces of primitive feather morphotypes, it may provide a new avenue for their detailed study.

4.3. Taphonomy

There are two potential interpretations for the selective preservation of body parts in HPG-15-1. The body may have been subject to predation or scavenging, or it may have been partially weathered away prior to full encapsulation in resin. The presence of undistorted outlines for body regions that are no longer supported by bones in HPG-15-1, suggests that predation or large-scale scavenging is unlikely to have produced the remains observed. The only feature that would support this interpretation is the offset position of the poorly preserved proximal femur (Fig. 1a, c). Given the jagged truncation of the central portion of the wing, it seems more likely that the corpse was partially embedded within a resin flow, and exposed areas were selectively removed. In this scenario, the parts of the bird that were not deeply buried within the resin flow were abraded, scavenged, decayed, or swept away by subsequent resin flows, leaving only a thin sheet of skin to represent most of the right side of the body. This sheet of skin and deeply embedded skeletal remains were then fully encapsulated by subsequent flows (Figs. S1, S2). The weathering scenario seems more likely, based on the drying lines visible within the surrounding amber. These indicate that much of the amber mass was produced by a single resin flow (with only one prominent drying line), and that this was repeatedly overlain by smaller resin flows. There are small, chevron-shaped distortions within the main resin flow containing skeletal material, but it is unclear whether these might be struggle marks, or lines imparted by the body sinking through the surrounding resin.

5. Conclusions

HPG-15-1 provides the first view of multiple body regions from an enantiornithine preserved in amber, including numerous diagnostic skeletal structures. It also provides the most comprehensive view of Cretaceous hatchling plumage known to date. The molt progression frozen within this piece of amber allows us to narrow down the potential age range for this specimen with a high degree of certainty, providing a point for comparisons to fossils in sedimentary rocks, and some of the isolated feathers from Cretaceous ambers. Ultimately, preservation in amber provides a clear view of feathers that have been difficult to interpret in compression fossils. Such clarity provides insight into which

structures are taphonomic in origin, and which unusual feather morphotypes may better inform our understanding of feather evolution. Hopefully, Burmese amber will continue to produce early avians in a wider range of taxa and life stages, so that this picture can be expanded.

Supplementary data to this article can be found online at <http://dx.doi.org/10.1016/j.gr.2017.06.001>.

Author contributions

L.X., J.O., R.M., B.M., designed the project, L.X., J.O., R.M., L.C., G.L., K.T., and B.M. performed the research, and L.X., J.O., L.C., R.M., and B.M. wrote the manuscript.

Acknowledgements

We thank CHEN Guang (Tengchong City Amber Association, Yunnan Province, China) for providing the specimen for study, Danae Frier and Ray Poulin (RSM), for study skin help and discussions; YANG Haidong and YIN Yideng for photographic contributions, and reviewers for constructive comments on an early version of this paper. This research was funded by the National Basic Research Program of China (973 Project: 2012CB822000); Natural Sciences and Engineering Research Council of Canada (2015-00681), the National Geographic Society, USA (EC0768-15); National Natural Science Foundation of China (No. 31672345, Special Subjects in Animal Taxonomy, NSFC-J1210002), Scientific Research Equipment Development Project of Chinese Academy of Sciences (YZ201509).

References

- Alonso, P.D., Milner, A.C., Ketchum, R.A., Cookson, M.J., Rowe, T.B., 2004. The avian nature of the brain and inner ear of *Archaeopteryx*. *Nature* 430, 666–669.
- Chiappe, L.M., 1993. Enantiornithine (Aves) tarsometatarsi from the Cretaceous Lecho Formation of northwestern Argentina. *American Museum Novitates* 3083, 1–27.
- Chiappe, L.M., 1996. Late Cretaceous birds of southern South America: anatomy and systematics of Enantiornithes and *Patagopteryx deferariisi*. *Münchner Geowissenschaftliche Abhandlungen* 30, 203–244.
- Chiappe, L.M., Calvo, J.O., 1994. *Neuquenornis volans*, a new late Cretaceous bird (Enantiornithes: Avisauridae) from Patagonia, Argentina. *Journal of Vertebrate Paleontology* 14, 230–246.
- Chiappe, L.M., Walker, C.A., 2002. Skeletal morphology and systematics of the Cretaceous Euenantiornithes (Ornithothoraces: Enantiornithes). In: Chiappe, L.M., Witmer, L.M. (Eds.), *Mesozoic Birds: Above the Heads of Dinosaurs*. University of California Press, Berkeley, pp. 240–267.
- Chiappe, L.M., Norell, M., Clark, J., 2001. A new skull of *Gobipteryx minuta* (Aves: Enantiornithes) from the Cretaceous of the Gobi Desert. *American Museum Novitates* 3346, 1–15.
- Chiappe, L.M., Ji, S., Ji, Q., 2007. Juvenile birds from the Early Cretaceous of China: implications for enantiornithine ontogeny. *American Museum Novitates* 3594, 1–49.
- Chinsamy, A., Elzanowski, A., 2001. Bone histology: evolution of growth pattern in birds. *Nature* 412, 402–403.
- Chinsamy, A., Chiappe, L.M., Dodson, P., 1995. Mesozoic avian bone microstructure: physiological implications. *Paleobiology* 21, 561–574.
- Cruikshank, R.D., Ko, K., 2003. Geology of an amber locality in the Hukawng Valley, northern Myanmar. *Journal of Asian Earth Sciences* 21, 441–455.
- Dal Sasso, C., Signore, M., 1998. Exceptional soft-tissue preservation in a theropod dinosaur from Italy. *Nature* 392, 383–387.
- Daza, J.D., Stanley, E.L., Wagner, P., Bauer, A.M., Grimaldi, D.A., 2016. Mid-Cretaceous amber fossils illuminate the past diversity of tropical lizards. *Science Advances* 2 (3), e1501080.
- Dhouailly, D., 2009. A new scenario for the evolutionary origin of hair, feather, and avian scales. *Journal of Anatomy* 214, 587–606.
- Dove, C.J., 2000. A descriptive and phylogenetic analysis of plumulaceous feather characters in Charadriiformes. *Ornithological Monographs* 51, 1–163.
- Elzanowski, A., 1981. Embryonic bird skeletons from the Late Cretaceous of Mongolia. *Palaeontologica Polonica* 42, 147–179.
- Foth, C., 2011. The morphology of neoptile feathers: ancestral state reconstruction and its phylogenetic implications. *Journal of Morphology* 272, 387–403.
- Gill, F.B., 2007. *Ornithology*. 3rd Edition. W.H. Freeman and Company, New York.
- Grimaldi, D.A., Engel, M.S., Nascimbene, P.C., 2002. Fossiliferous Cretaceous amber from Myanmar (Burma): its rediscovery, biotic diversity, and paleontological significance. *American Museum Novitates* 3361, 1–72.
- Hu, H., O'Connor, J.K., 2016. First species of Enantiornithes from Sihedang elucidates skeletal development in Early Cretaceous enantiornithines. *Journal of Systematic Palaeontology* 1–18.
- Kaiser, G.W., Dyke, G.J., 2010. Cracking a developmental constraint: egg size and bird evolution. *Records of the Australian Museum* 62, 207–216.
- Kurochkin, E.N., 1996. A new enantiornithid of the Mongolian Late Cretaceous, and a general appraisal of the Infraclass Enantiornithes (Aves). Special Issue. Russian Academy of Sciences, Palaeontological Institute, pp. 1–50.
- Kurochkin, E.N., Chatterjee, S., Mikhailov, K.E., 2013. An embryonic enantiornithine bird and associated eggs from the Cretaceous of Mongolia. *Paleontological Journal* 47, 1252–1269.
- Lucas, A.M., Stettenheim, P.R., 1972. *Avian Anatomy: Integument*. US Government Printing Office, Washington.
- Martínez-Delclòs, X., Briggs, D.E., Peñalver, E., 2004. Taphonomy of insects in carbonates and amber. *Palaeogeography, Palaeoclimatology, Palaeoecology* 203, 19–64.
- Mayr, G., 2016. Evolution of avian breeding strategies and its relation to the habitat preferences of Mesozoic birds. *Evolutionary Ecology*:1–11 <http://dx.doi.org/10.1007/s10682-016-9872-1>.
- Mayr, G., Pohl, B., Hartman, S., Peters, D.S., 2007. The tenth skeletal specimen of *Archaeopteryx*. *Zoological Journal of the Linnean Society* 149, 97–116.
- Murphy, N.L., Trexler, D., Thompson, M., 2006. “Leonardo,” a mummified *Brachylophosaurus* from the Judith River Formation. In: Carpenter, K. (Ed.), *Horns and Beaks: Ceratopsian and Ornithopod Dinosaurs*. Indiana University Press, Bloomington, pp. 117–133.
- O'Connor, J., 2012. A revised look at *Liaoningornis longidigitrus* (Aves). *Vertebrata Palasiatica* 5, 25–37.
- O'Connor, J., Chiappe, L.M., 2011. A revision of enantiornithine (Aves: Ornithothoraces) skull morphology. *Journal of Systematic Palaeontology* 9, 135–157.
- O'Connor, J.K., Chiappe, L.M., Bell, A., 2011. Pre-modern birds: avian divergences in the Mesozoic. In: Dyke, G.D., Kaiser, G. (Eds.), *Living Dinosaurs: The Evolutionary History of Birds*. J. Wiley & Sons, Hoboken, NJ, pp. 39–114.
- O'Connor, J.K., Wang, M., Zheng, X.T., Wang, X.L., Zhou, Z.H., 2014. The histology of two female Early Cretaceous birds. *Vertebrata Palasiatica* 52, 113–128.
- Osborn, H.F., 1912. Integument of the iguanodont dinosaur *Trachodon*. *Memoirs of the American Museum of Natural History*, 1(2) New Series, pp. 33–54.
- Ossa-Fuentes, L., Mpodozis, J., Vargas, A.O., 2015. Bird embryos uncover homology and evolution of the dinosaur ankle. *Nature Communications* 6, 1–7.
- Prum, R.O., 1999. Development and evolutionary origin of feathers. *Journal of Experimental Zoology* 285, 291–306.
- Ricklefs, R.E., 1973. Patterns of growth in birds. II. Growth rate and mode of development. *Ibis* 115, 177–201.
- Ross, A., Mellish, C., York, P., Crighton, B., 2010. Burmese amber. In: Penney, D. (Ed.), *Biodiversity of Fossils in Amber from the Major World Deposits*. Siri Scientific Press, Manchester, pp. 208–235.
- Sanz, J.L., Chiappe, L.M., Pérez-Moreno, B., Moratalla, J.J., Hernández-Carrasquilla, F., Buscalioni, A.D., Ortega, F., Poyato-Ariza, F.J., Rasskin-Gutman, D., Martínez-Delclòs, X., 1997. A nestling bird from the Lower Cretaceous of Spain: implications for avian skull and neck evolution. *Science* 276, 1543–1546.
- Sanz, J.L., Chiappe, L.M., Fernández-Jalvo, Y., Ortega, F., Sánchez-Chillón, B., Poyato-Ariza, F.J., Pérez-Moreno, B.P., 2001. Palaeontology: an Early Cretaceous pellet. *Nature* 409, 998–1000.
- Schweitzer, M.H., Jackson, F.D., Chiappe, L.M., Schmitt, J.G., Calvo, J.O., Rubilar, D.E., 2002. Late Cretaceous avian eggs with embryos from Argentina. *Journal of Vertebrate Paleontology* 22, 191–195.
- Shi, G., Grimaldi, D.A., Harlow, G.E., Wang, J., Wang, J., Yang, M., Lei, W., Li, Q., Li, X., 2012. Age constraint on Burmese amber based on U–Pb dating of zircons. *Cretaceous Research* 37, 155–163.
- de Souza Carvalho, I., Novas, F.E., Agnolin, F.L., Isasi, M.P., Freitas, F.I., Andrade, J.A., 2015. A Mesozoic bird from Gondwana preserving feathers. *Nature Communications* 6, 1–5.
- Starck, J.M., 1993. Evolution of avian ontogenies. *Current Ornithology* 10, 275–366.
- Starck, J.M., Ricklefs, R.E., 1998. Patterns of development: the altricial-precocial spectrum. In: Starck, J.M., Ricklefs, R.E. (Eds.), *Avian Growth and Development*. Oxford University Press, New York City, pp. 3–30.
- Wang, X.-L., O'Connor, J.K., Zheng, X.-T., Wang, M., Hu, H., Zhou, Z.-H., 2014. Insights into the evolution of rachis dominated tail feathers from a new basal enantiornithine (Aves: Ornithothoraces). *Biological Journal of the Linnean Society*, London 113, 805–819.
- Wang, M., Hu, H., Li, Z.-H., 2016a. A new small enantiornithine bird from the Jehol Biota, with implications for early evolution of avian skull morphology. *Journal of Systematic Palaeontology* 14, 481–497.
- Wang, S., Shi, C., Zhang, Y.-J., Huo, G.-X., Gao, L.-Z., 2016b. Trading away ancient amber's secrets. *Science* 351, 926.
- Wong, S., 1999. *Development and Behaviour of Hatchlings of the Australian Brush-turkey *Alectura lathami**. (PhD Dissertation). Griffith University, Brisbane.
- Xing, L., Bell, P.R., Persons IV, W.S., Ji, S., Miyashita, T., Burns, M.E., Ji, Q., Currie, P.J., 2012. Abdominal contents from two large Early Cretaceous compsognathids (Dinosauria: Theropoda) demonstrate feeding on confuciosornithids and dromaeosaurids. *PLoS One* 7 (8), e44012.
- Xing, L.-D., McKellar, R.C., Wang, M., Bai, M., O'Connor, J.K., Benton, M.J., Zhang, J.-P., Wang, Y., Tseng, K.-W., Lockley, M., Li, G., Zhang, W.-W., Xu, X., 2016a. Mummified precocial bird wings in mid-Cretaceous Burmese amber. *Nature Communications* 7: 12089. <http://dx.doi.org/10.1038/ncomms12089>.
- Xing, L.-D., McKellar, R.C., Xu, X., Li, G., Bai, M., Persons, W.S., Miyashita, T., Benton, M.J., Zhang, J.-P., Wolfe, A.P., Yi, Q.-R., Tseng, K.-W., Ran, H., Currie, P.J., 2016b. A feathered dinosaur tail with primitive plumage trapped in mid-Cretaceous amber, and its implications for the evolution of feathers. *Current Biology* 26, 3352–3360.
- Zheng, X.-T., Wang, X.-L., O'Connor, J.K., Zhou, Z.-H., 2012. Insight into the early evolution of the avian sternum from juvenile enantiornithines. *Nature Communications* 3, 1–8.

- Zheng, X.-T., O'Connor, J.K., Huchzermeyer, F.W., Wang, X.-L., Wang, Y., Wang, M., Zhou, Z.-H., 2013. Preservation of ovarian follicles reveals early evolution of avian reproductive behaviour. *Nature* 495, 507–511.
- Zhou, Z., Zhang, F., 2004. A precocial avian embryo from the Lower Cretaceous of China. *Science* 306, 653.
- Zhou, Z., Barrett, P.M., Hilton, J., 2003. An exceptionally preserved Lower Cretaceous ecosystem. *Nature* 421, 807–814.
- Zhou, Z., Clarke, J., Zhang, F., 2008. Insight into diversity, body size and morphological evolution from the largest Early Cretaceous enantiornithine bird. *Journal of Anatomy* 212, 565–577.